CEA DSM DAPNIA SACM

report CEA DSM DAPNIA/SEA-00-02

CERN-NUFACT-Note-0106

On the effects of fringe fields in the CERN 50 GeV muon storage ring

F. Méot
CEA DSM/DAPNIA/SACM, 91191 Saclay, France
(fmeot@cea.fr)

Abstract

This paper examines possible effects (or non-effects) of magnet fringe fields in the CERN 50 GeV muon storage ring project. This is done by means of classical multiturn tracking methods, based on stepwise ray-tracing. Comparisons with earlier studies are performed.

February 1, 2002

Contents

1 Introduction **3**

2 The treatment of fringe fields **3**

3 Linear machine - basic optical properties 4
3.1 Optical parameters 5
3.2 Transverse motion 5
3.3 Chromatism 6

4 Assessment of fringe fields effects **6**
4.1 Quadrupole fringe field 8
4.1.1 Optical parameters 8
4.1.2 Multiturn ray-tracing 11
4.2 Bend fringe field 11

5 Chromatic effects - sextupoles off **13**

6 Chromaticity corrected machine **15**
6.1 Fringe fields in quadrupoles only 16
6.2 Fringe fields in bends and quadrupoles 19

7 6-D dynamic aperture **22**

8 Comparisons with PEP magnets fringe field **24**
8.1 Fringe fields in quadrupoles only 24
8.2 Fringe fields in bends and quadrupoles 27

9 Conclusion **27**

Appendix **29**

A MAD data file **29**

B Zgoubi data file **30**

C Fringe fields in bends with GSI and PEP coefficients **30**

D Remarks on the design of fringe fields **31**

References **33**

1 Introduction

Possible effects of magnet fringe fields on various machine parameters and on dynamic and momentum acceptance in the CERN 50 GeV muon storage ring [1] are investigated by means of multiturn stepwise ray-tracing, according to working hypothesis of an earlier detailed study performed with the computer code COSY [2].

The paper may seem lengthy, this is because we proceed step by step, switching fringe fields separately in various types of elements in order to appreciate where causes are. However most of the surface is occupied by graphs and tables.

Unless otherwise mentioned, working conditions, design parameters, etc., refer to Refs. [1] and [2], whose data can be readily compared to the present ones. Additional MAD [3] simulations are presented in due place in order to provide comparisons and to help clarifying to what extent fringe field induced non-linearities have (or do not have) sensible effect.

The report is organized as follows :
Section 2 describes briefly the Zgoubi method. Section 3 establishes the basic optical properties of the storage ring on the basis of that method, for reference and possible comparisons with MAD or other codes. Sections 4-6 introduce one after the other additional ingredients such as fringe fields, chromatic corrections and so forth, from the bare lattice to the complete case of concern. Section 7 concludes that all by a 6-D dynamic aperture (DA) tracking with nominal beam emittances. Eventually Section 8 shows that fringe field coefficients used in Ref. [2] lead to similar results.

Various Appendices give additional details concerning numerical data and methods used in these simulations, for reference.

2 The treatment of fringe fields

The ray-tracing code utilized [4, 5] allows accurate simulation of longitudinal or transverse non-linearities and their effect on particle motion, hence giving access with precision to usual first and higher order machine parameters as well as dynamic aperture calculations.

The integration method is based on stepwise resolution of Lorentz equation by a technique of Taylor series ; details can be found in Ref. [4], aspects relevant to the present study are recalled hereafter. Several problems related to the design of circular machines have been subject to published similar studies that can be referred to for more details on the technic [6]-[8].

Simulation of multipole fields Explicit analytical expressions of multipole fields and of their derivatives are used in the integration algorithm, they derive from the regular 3-D scalar potential model [9]

$$V_n(s,x,y) = (n!)^2\{\sum_{q=0}^{\infty}(-)^q\frac{\alpha_{n,0}^{(2q)}(s)}{4^q q!(n+q)!}(x^2+y^2)^q\}\{\sum_{m=0}^{n}\frac{sin(m\frac{\pi}{2})x^{n-m}y^m}{m!(n-m)!}\} \qquad (1)$$

which in the case of the dipole and quadrupole components of concern in the muon ring magnets takes the explicit forms

$$V_1(s,x,y) = \alpha_{1,0}(s)y - \frac{\alpha^{(2)}_{1,0}(s)}{8}(x^2+y^2)y + \frac{\alpha^{(4)}_{1,0}(s)}{192}(x^2+y^2)^2 y - ... \qquad (2)$$

$$V_2(s,x,y) = \alpha_{2,0}(s)xy - \frac{\alpha^{(2)}_{2,0}(s)}{12}(x^2+y^2)xy + \frac{\alpha^{(4)}_{2,0}(s)}{384}(x^2+y^2)^2 xy - ... \qquad (3)$$

where s, x, y coordinates are respectively curvilinear, transverse horizontal and vertical, $\alpha_{n,0}(s)$ ($n = 1,2,3, etc.$) describe the longitudinal form of the field, including end fall-offs, with $\alpha^{(2q)}_{n,0} = d^{2q}\alpha_{n,0}/ds^{2q}$. Note that, within magnet body or as well when using hard edge field model, $d^{2q}\alpha_{n,0}/ds^{2q} \equiv 0$ ($\forall q \neq 0$) and hence the field and derivatives derive from the simplified potentials

$$V_1(x,y) = G_1 y, \quad V_2(x,y) = G_2 xy \qquad (4)$$

where $G_n/B\rho$ is the strength.

Field fall-off at magnet ends As to the field fall-off on axis at magnet ends orthogonally to the effective field boundary (*EFB*), it is modeled by [10, page 240]

$$\alpha_{n,0}(d) = \frac{G_n}{1+\exp[P(d)]} \quad \text{with} \quad P(d) = C_0 + C_1\frac{d}{\lambda_n} + C_2(\frac{d}{\lambda_n})^2 + \ ... \ + C_5(\frac{d}{\lambda_n})^5 \qquad (5)$$

where d is the distance to the *EFB* and coefficients λ_n, $C_0 - C_5$ can be determined from prior matching with numerical fringe field data. The interest of λ_n is that it can be varied at will to possibly change or test the effect of the fall-off abruptness, without affecting the position of the *EFB* (i.e., without any effect on the magnetic length).

3 Linear machine - basic optical properties

We here set the basis material concerning the storage ring prior to investigating fringe fields, by first producing and checking main parameters of the linear machine (i.e., no fringe fields - Eq. 4 holds, and sextupoles off).

In addition, it can be drawn from what follows, from the similarity between MAD and ray-tracing results, that possible kinematic terms have negligible effect within the machine physical acceptance.

In order that there be no doubt as to which optical structure is effectively dealt about in the following, and to allow further comparison with ray-tracing results, let us first give relevant outputs of MAD simulations (data file given in App. A) :

MAD outputs

```
Periodic optical functions at the origin of the structure :

-----------------------------------------------------------------------------------------------
   ELEMENT SEQUENCE I        H O R I Z O N T A L          I            V E R T I C A L
pos.  element occ.  I   betax  alfax   mux     Dx    Dpx  I   betay  alfay   muy    Dy    Dpy
no.   name    no.   I   [m]    [1]     [2pi]   [m]   [1]  I   [m]    [1]     [2pi]  [m]   [1]
```

```
------------------------------------------------------------------------------------------------
begin SMSR       1    249.649   .000    .000    .000  .000  115.321   .000    .000    .000  .000
end   SMSR       1    249.649   .000  11.254    .000  .000  115.321   .000  12.287    .000  .000
------------------------------------------------------------------------------------------------
total length = 2068.759047         Qx           =   11.254455          Qy           =   12.287298
delta(s)     =     .000000 mm      Qx'          =  -17.403507          Qy'          =  -17.443769
alfa         =     .258663E-02     betax(max)   =  258.354052          betay(max)   =  249.649089
------------------------------------------------------------------------------------------------
------------------------------------------------------------------------------------------------
HARMON startup.              HARMON              line: SMSR                       range: #S/#E
Delta(p)/p:      .000000     symm: F             super:   1
------------------------------------------------------------------------------------------------
Derivatives of tune w.r.t. momentum:
                h o r i z o n t a l                              v e r t i c a l
          first          second           third          first          second           third
   -1.748398E+01   -7.893065E+00    3.599541E+04   -1.736346E+01   -2.168948E+02    3.378609E+04

Tune shift with amplitude:
     d(Qx)/d(Ex)     d(Qy)/(dEy)     d(Qy)/d(Ex)
    0.000000E+00    0.000000E+00    0.000000E+00
```

3.1 Optical parameters

MAD data nomenclature will be adopted in the rest of the text, e.g., "*SMSR*" for designating the origin of the structure, Q_x, Q_y for tunes, etc. For comparison, the ray-tracing of paraxial rays[1] results in (typical data file given in App. B) :

Zgoubi results

```
         Structure  length : 206875.960  cm

                Beam matrix and periodic dispersion at SMSR ( MKSA )

       249.649717     -.000001      .000000      .000000      .000018 = D_X
         -.000001      .004006      .000000      .000000      .000000 = D'_x
          .000000      .000000   115.320920      .000004
          .000000      .000000      .000004      .008671

           NUX =      .25446672      NUY =      .28720015
```

Comparison between MAD and ray-tracing simulations above show very good similarity at first order, in the case of the (fringe field free) linear machine.

3.2 Transverse motion

Ray-tracing provides beam envelopes shown in Fig. 1, that permit checking the correct behavior of the method up to the maximum geometrical aperture (for simplicity we consider equal limits $\approx 9\ 10^{-2}$m in both planes at *SMSR*), and comparison with analogous MAD plots in Ref. [1, page 10, Fig. 9]. Fig. 2 shows sample phase space trajectories at *SMSR* that reveal (Table 1) on the one hand - from elliptical fit, x_0- and y_0-independent beta values, on the other hand - from Fourier analysis, negligible amplitude detuning (zero is expected in the paraxial case), namely, using $\epsilon_x/\pi(x_0 = 0.01$ m$) \approx 4\ 10^{-7}$ m.rad and

[1] Zgoubi derives transfer coefficients and other Twiss parameters from polynomial interpolation based on the ray-tracing of *ad hoc* sets of paraxial rays.

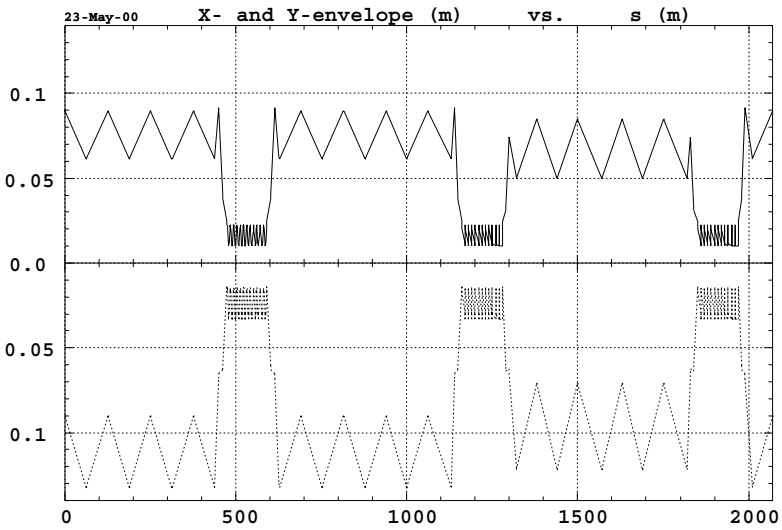

Figure 1: Horizontal (solid line) and vertical (dashed line) envelopes in the muon storage ring corresponding to x_0 and $y_0 = 9\ 10^{-2}$m at *SMSR*, as generated from ray-tracing. Sextupoles are off, no fringe fields.

$\epsilon_y/\pi(y_0 = 0.01\text{ m}) \approx 8.7\ 10^{-7}$ m.rad with $Q_{x,y}$ values of Table 1,

$$dQ_x/d\epsilon_x/\pi = -37\ , \qquad dQ_y/d\epsilon_y/\pi = -2.3 \tag{6}$$

3.3 Chromatism

Table 2 gives sample beta values at *SMSR* and momentum detuning within $|\delta| \leq 1\%$ obtained from 1000-turn ray-tracing. Particles have been launched with $x_0 = 0$ which practically places them on the chromatic closed orbit since D_x and $D'_x \approx 0$ at *SMSR*, and with very small vertical amplitude in order to be able to (while avoiding $x - y$ coupling) derive local β_y values from ellipse fit, and vertical tunes from Fourier analysis. One can notice that going beyond $\delta \approx 6\ 10^{-3}$ is of little meaning in terms of betatron amplitudes, yet it serves our comparison in the linear limit. Chromaticities drawn from Table 2 are (Zgoubi/MAD)

$$\begin{aligned} Q'_x = -17.40\ /\ -17.50\ , \qquad & Q'_y = -17.45\ /\ -17.32 \\ Q''_x = 38\ /\ 38\ , \qquad & Q''_y = 27\ /\ 27 \end{aligned} \tag{7}$$

4 Assessment of fringe fields effects

In this Section we reconsider calculations of various parameter and graphs, with fringe fields set in bends, or quadrupoles, or both types of magnets as indicated, while keeping sextupoles off.

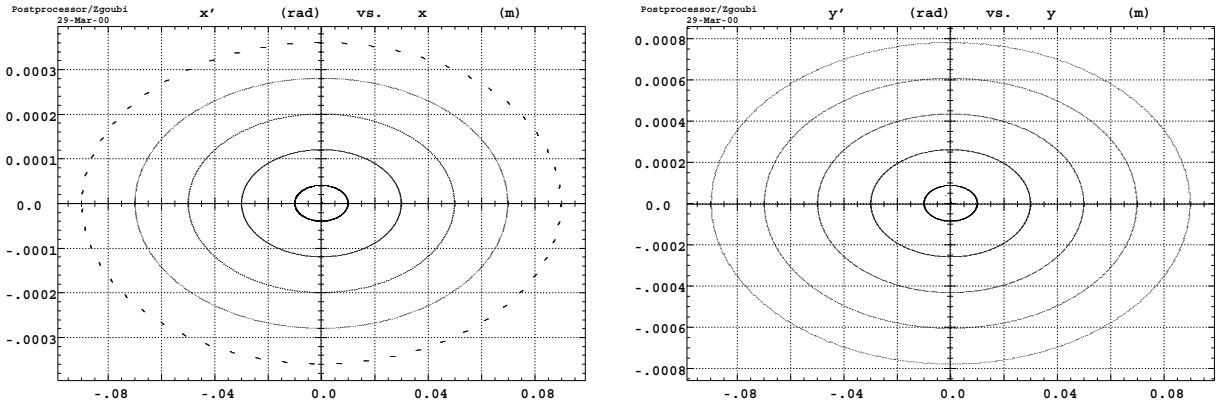

Figure 2: Phase space trajectories observed at *SMSR*. No fringe fields. Sextupoles are off. 1000-turn ray-tracing. Initial conditions were respectively,
left : $x_0 = 1 - 9 \times 10^{-2}$m and $\epsilon_y = 0$ and,
right : $y_0 = 1 - 9 \times 10^{-2}$m and $\epsilon_x = 0$.
All particles survive.

Table 1: Amplitude detuning as obtained from Fourier transform of the 1000-turn phase space coordinates displayed in Fig. 2, and beta values at *SMSR* as obtained from their ellipse fitting.

Amplitude detuning - linear machine, no fringe fields					
Horizontal ($\epsilon_y = 0$)			Vertical ($\epsilon_x = 0$)		
x_0 (10^{-2}m)	Q_x fractional	β_x (m) at *SMSR*	y_0 (10^{-2}m)	Q_y fractional	β_y (m) at *SMSR*
0.001	.254465	249.6	0.001	.287200	115.2
1	.254450	249.6	1	.287198	115.2
5	.254491	249.6	5	.287253	115.2
9	.254553	249.6	9	.287370	115.3

Table 2: Momentum detuning. Comparison Zgoubi/MAD.

Momentum detuning - linear machine, no fringe fields				
$\delta p/p$	Horizontal		Vertical	
	Q_x fractional	β_x (m) at *SMSR*	Q_y fractional	β_y (m) at *SMSR*
	Zgoubi/MAD		Zgoubi/MAD	
-0.01	.431501 /.432809	255.39/255.72	.468368 /.466929	196.00 /191.82
-0.006	.359808 /.360589	247.48/247.53	.392891 /.392178	125.30/125.22
-0.002	.289360 /.289613	247.70 /247.71	.322159 /.321990	116.76/116.76
0.	.254467/.254455	249.64/249.64	.287200 /.287298	115.32/115.32
0.002	.219728 /.219448	253.03/253.03	.252349 /.252714	114.82/114.82
0.006	.150424 /.149600	267.11/267.25	.182450 /.183352	116.48/116.44
0.01	.080140 /.078722	313.34/314.75	.110260 /.111755	126.17/125.88 /

4.1 Quadrupole fringe field

Fringe fields are first set in part of, or all quadrupoles, as indicated.

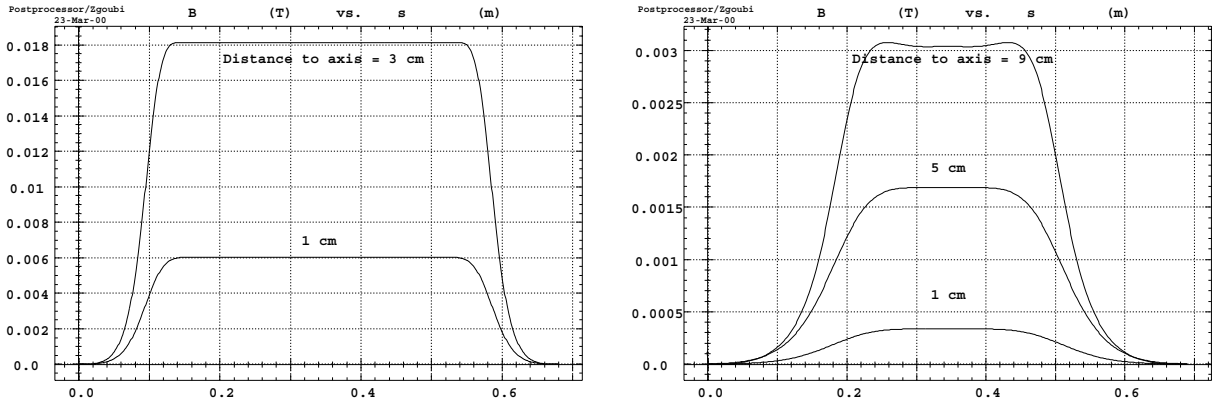

Figure 3: Left : magnetic field $B(s)$ observed in the arc quadrupoles 1 and 3×10^{-2}m off-axis and, right : in the straight section quadrupoles (as well as, apart from the overall length, in the matching sections quadrupoles) 1, 5 and 9×10^{-2}m off-axis.

We account for two forms of longitudinal fall-offs, one type for the about 9×10^{-2}m radius quadrupoles of the long straight and matching sections, another type for the about 3×10^{-2}m radius arc quadrupoles. Both are based on the same set of Enge coefficients[2]

$$C_0 = 0.1122,\ C_1 = 6.2671,\ C_2 = -1.4982,\ C_3 = 3.5882,\ C_4 = -2.1209,\ C_5 = 1.723 \quad (8)$$

and they only differ by the scaling factor $\lambda_2 = 0.2$ m or 0.09 m respectively. Figure 3 displays the so-obtained longitudinal shape of the field in both types of quadrupoles at various radii within their geometrical aperture. There is some arbitrariness in this choice of λ_2 values, our goal being that fall-off smoothness be preserved over the all geometrical aperture whereas, considering concluding remark in Section 2 (page 4), changing λ_2 is innocuous as to the first order focusing.

Earlier studies would allow analytical calculation of quadrupole fringe fields induced tune shift and momentum coupled tune shift, given the first order optics and longitudinal fall-off gradient derivatives [12].

4.1.1 Optical parameters

Comparison between the three cases of beam matrices below, and Zgoubi/MAD results of Section 3.1 show slight change w.r.t. the fringe field free machine, in particular in tune values.

[2]Values arbitrarily drawn from former design of a warm, non-saturated 0.15 m radius spectrometer quadrupole at GSI [11], subject to 3-D TOSCA calculations and magnetic measurements ; they are believed to be representative of our concern. Another extreme would be the end field of the LHC superconducting arc quadrupole (see Ref. [7]) with adequate λ_2 scaling, yet with possibly little difference as to non-linear effects - this point is also addressed in Section 8.

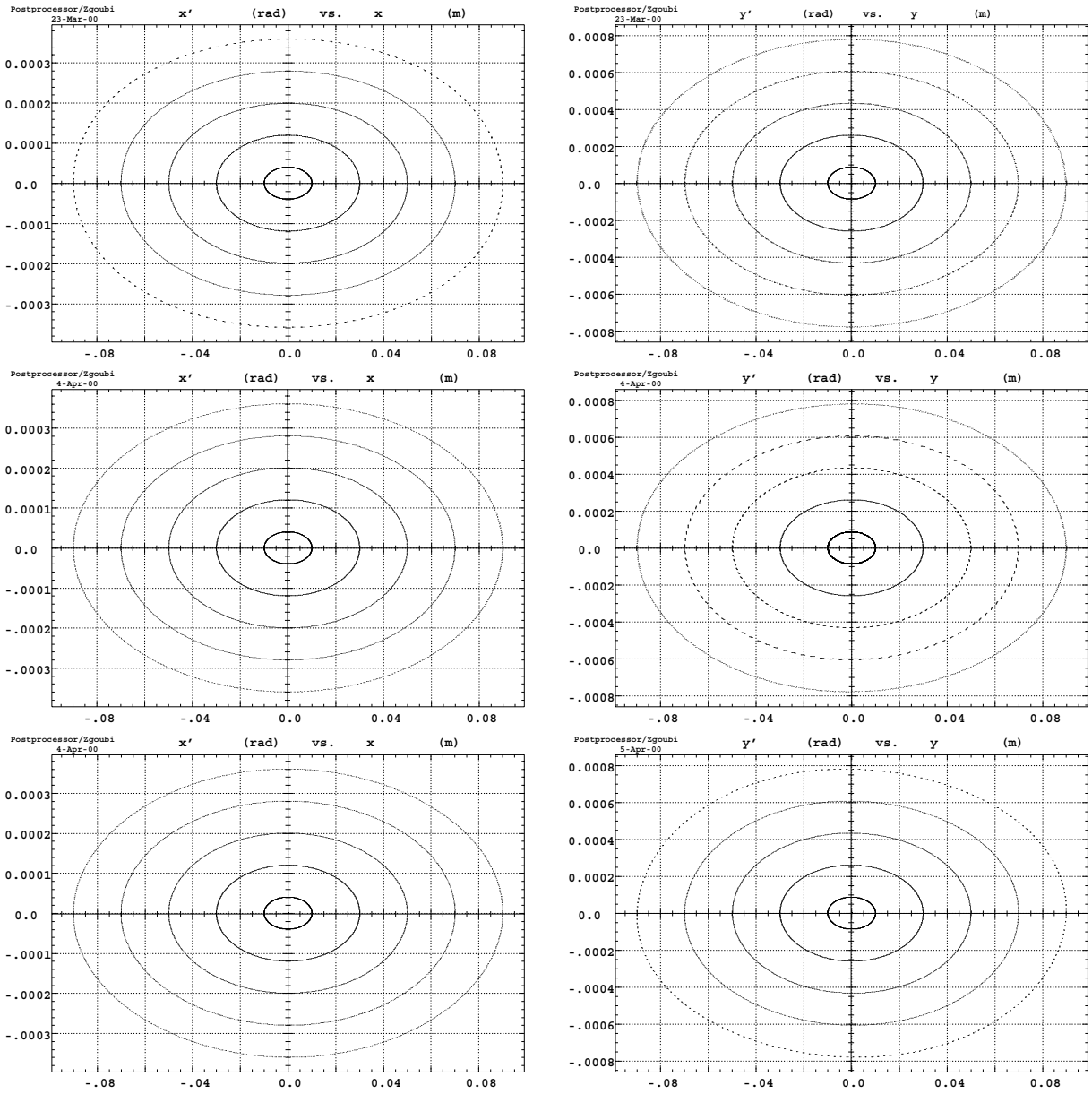

Figure 4: Horizontal (left) and vertical (right) phase spaces observed at *SMSR*. Sextupoles are off. 1000-turn ray-tracing. Initial conditions were respectively,
left : $x_0 = 1 - 9 \times 10^{-2}$m by 10^{-2}m steps and $y_0 \equiv 0$, and
right : $y_0 = 1 - 9 \times 10^{-2}$m by 10^{-2}m steps and $x_0 \equiv 0$.
- Top row : fringe fields are set in all quadrupoles.
- Middle row : fringe fields are set in bends only.
- Bottom row : fringe fields are set in bends and all quadrupoles.
All particles survive.

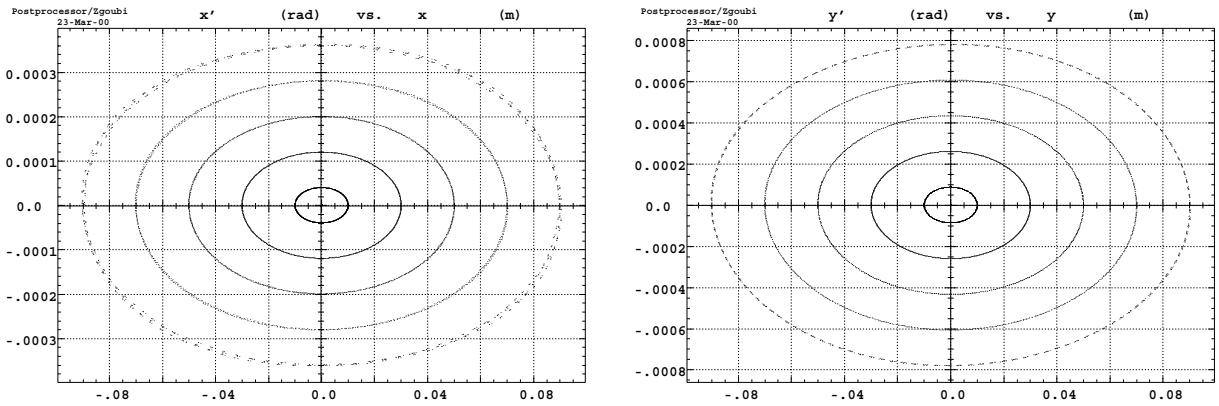

Figure 5: Same as Fig. 4-top except for diagonal initial conditions $x_0 = y_0 = 1 - 9 \times 10^{-2}$m by 10^{-2}m steps. All particles survive.

Ray-tracing results

Fringe fields set in all quadrupoles :

```
          Beam matrix and periodic dispersion at SMSR ( MKSA )

251.124756     -.002316      .000000      .000000      .015720
  -.002316      .003982      .000000      .000000      .000047
   .000000      .000000   115.206812     -.005539
   .000000      .000000     -.005539      .008680

   NUX =      .23506567      NUY =      .27000987
```

Fringe fields set in straight and matching sections quadrupoles only :

```
          Beam matrix and periodic dispersion at SMSR ( MKSA )

251.827870     -.003271      .000000      .000000      .000025
  -.003271      .003971      .000000      .000000      .000000
   .000000      .000000   115.145034     -.005314
   .000000      .000000     -.005314      .008685

   NUX =      .24475382      NUY =      .28047134
```

Fringe fields set in arc quadrupoles only :

```
          Beam matrix and periodic dispersion at SMSR ( MKSA )

248.811862      .001152      .000000      .000000      .015319
   .001152      .004019      .000000      .000000      .000047
   .000000      .000000   115.328814      .000211
   .000000      .000000      .000211      .008671

   NUX =      .24476049      NUY =      .27673812
```

It may not be useless to mention that beam matrices above and other results below are insured stability w.r.t. the integration step size, w.r.t. slight changes in λ_2 (Eqs. 3, 5), and as well w.r.t. to the initial coordinates of the paraxial rays (this kind of arguments are addressed in earlier similar works [6]-[8]).

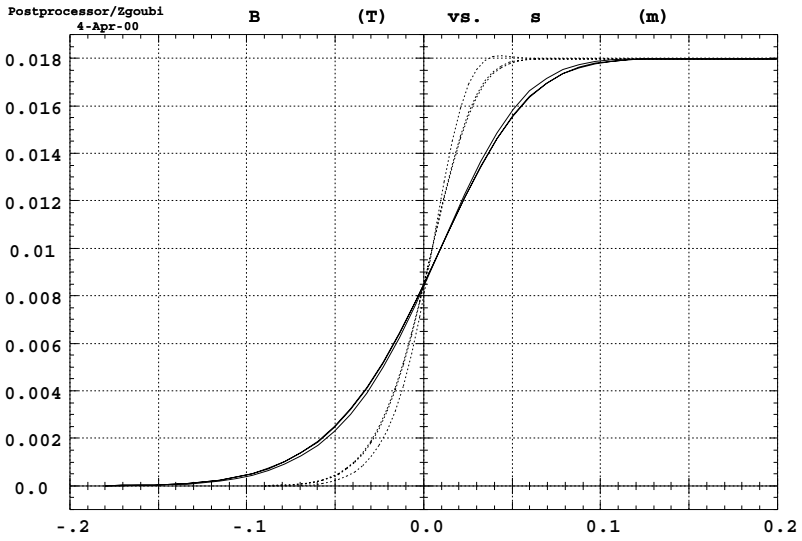

Figure 6: Fringe fields in bends, on- and 3 cm off-axis, with $\lambda_1 = 0.18$ m (solid line) and $\lambda_1 = 0.09$ m (dashed line).

4.1.2 Multiturn ray-tracing

Fig. 4-top shows phase space trajectories at *SMSR* obtained from a 1000-turn run, in the case of independent x_0 and y_0 initial conditions, with fringe fields set in all quadrupoles. The dynamic aperture with these working hypothesis appears to exceed the physical acceptance.

Table 3 gives the corresponding amplitude detuning. Fig. 5 is obtained similarly to Fig. 4-top but for the diagonal initial conditions $x_0 = y_0$; again the so-obtained dynamic aperture exceeds the physical acceptance.

4.2 Bend fringe field

As to the bends, the same field fall-off coefficients as in the arc quadrupoles are used (Eq. 8) while two values of the scaling factor λ_1 are considered, as indicated below ; they are displayed in Fig. 6.

Fringe fields in bends only Fig. 4-middle shows phase space trajectories at *SMSR* obtained from a 1000-turn run, in the case of independent x_0 and y_0 initial conditions, with fringe fields set in bends only and $\lambda_1 = 0.18$ m (twice λ_2 ; accessorily, the corresponding MAD coefficient takes the value $I1 \cdot gap = \int \alpha_{1,0}(s)(1-\alpha_{1,0}(s))\, ds = 0.0262$ m). Sensibility to the fall-off abruptness is assessed by running the same problem with $\lambda_1 = 0.09$ m ($I1 \cdot gap = 0.0131$ m) : quasi identical phase space is obtained, tunes increase slightly in both planes as shown in Table 3.

As a conclusion, the dynamic aperture with these working hypothesis appears to remain beyond physical acceptance.

Table 3: Amplitude detuning as obtained from Fourier transform of 1000-turn phase space coordinates at *SMSR* (Fig. 4), and related beta values.
Bend fringe fields with $\lambda_1 = 0.18$ and 0.09 m are shown in Fig. 6.

Amplitude detuning Arc sextupoles are off					
	Horizontal (ϵ_y=0)			Vertical (ϵ_x=0)	
x_0 (10^{-2}m)	Q_x fractional	β_x (m)	y_0 (10^{-2}m)	Q_y fractional	β_y (m)
Fringe fields set in all quads (Fig. 4-top)					
0.001	.235063		0.001	.270005	
1	.235111		1	.270083	
3	.235509		3	.270699	
5	.236280		5	.271825	
7	.237375		7	.273253	
9	.238713		9	.274484	
Fringe fields set in bends only (Fig. 4-middle)					
$\lambda_1 = 0.18$ *m*					
0.001	.287065		0.001	.252159	
1	.287066		1	.252162	
5	.287093		5	.252248	
9	.287153		9	.252440	
$\lambda_1 = 0.09$ *m*					
0.001	.287631		0.001	.252788	
1	.287643		1	.252801	
5	.287529		5	.253124	
9	.287285		9	.253829	
Fringe fields set in bends and quads (Fig. 4-bottom)					
$\lambda_1 = 0.18$ *m*					
0.001	.267674	250.5	0.001	.234950	115.3
1	.267725	250.6	1	.235037	115.3
5	.268892	250.2	5	.236820	115.4
9	.271301	249.9	9	.239631	115.4
$\lambda_1 = 0.09$ *m*					
0.001	.268266	250.3	0.001	.235577	115.3
1	.268309	250.4	1	.235669	115.2
5	.269343	250.4	5	.237699	115.4
9	.271421	249.8	9	.241081	115.2

Fringe fields in bends and all quadrupoles Beam matrix and tunes below can be compared to Sections 3.1 (p. 5) and 4.1.1 (p. 10).

```
          Beam matrix and periodic dispersion at SMSR ( MKSA )

 250.611631     -.001406      .000000      .000000      .000646
  -.001406      .003990      .000000      .000000      .000002
   .000000      .000000   115.363128     -.006403
   .000000      .000000     -.006403      .008669

    NUX =      .26827765      NUY =      .23559395    (lambda=0.09 m)
```

Fig. 4-bottom shows phase space trajectories at *SMSR* obtained from a 1000-turn run, in the case of independent x_0 and y_0 initial conditions, with fringe fields set in bends with $\lambda_1 = 0.18$ m and in all quadrupoles. The dynamic aperture with these working hypothesis appears to exceed the physical acceptance. Similar plots (not shown) are obtained with $\lambda_1 = 0.09$ m. Table 3 gives the corresponding tunes as a function of amplitude, together with the local value of the beta functions at *SMSR* that appear to be but weakly affected by fringe fields, as well.

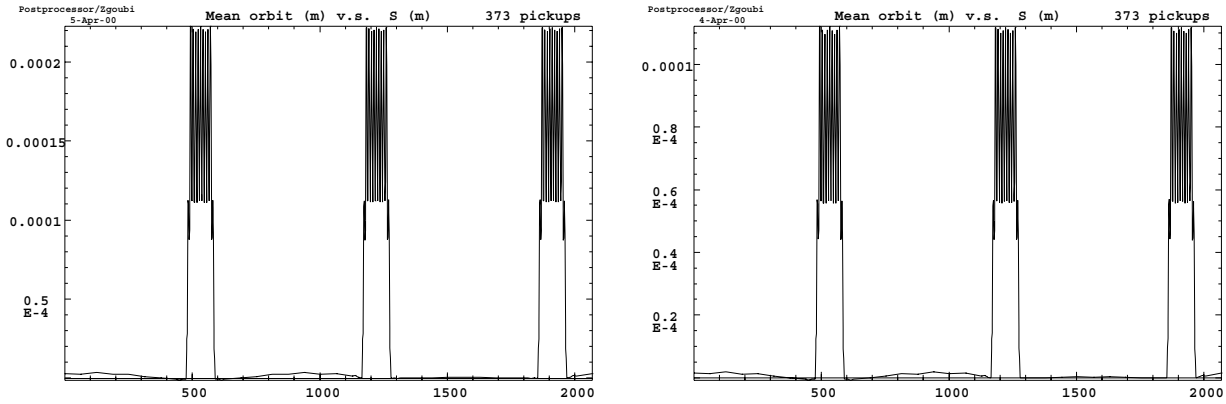

Figure 7: Geometrical closed orbit induced by bends fringe fields, for $\lambda_1 = 0.18$ m (left) and for $\lambda_1 = 0.09$ m (right). No fringe field in quadrupoles, sextupoles off.

Closed orbit Fringe fields in bends generate closed orbit [10]. As already studied in such machines as LHC [7] or Fermilab recycler ring [8] the effect is expected to be weak, as confirmed in Fig. 7 that displays closed orbits averaged from 100-turn pick-up signal, in both cases $\lambda_1 = 0.18$ m and $\lambda_1 = 0.09$ m.

5 Chromatic effects - sextupoles off

We now investigate momentum spread δ, fringe fields set in bends and quadrupoles, sextupoles still off. Fifteen particles are launched at *SMSR* with $-1.4\ 10^{-2} \leq \delta \leq 1.4\ 10^{-2}$, with zero initial horizontal coordinates since the local chromatic closed orbit is in principle zero, and very small amplitude vertical motion in order to be able to get the vertical tunes

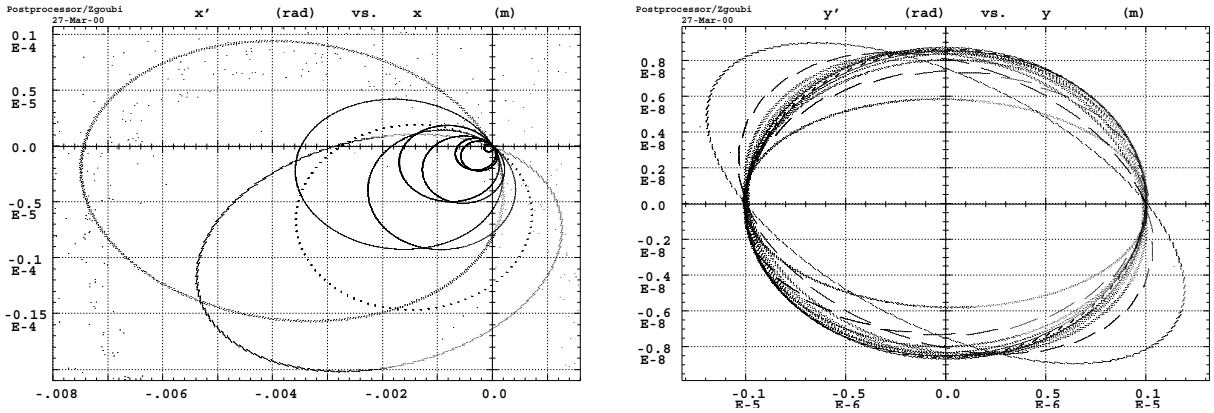

Figure 8: Horizontal (left) and vertical (right) phase space trajectories at *SMSR* of particles launched on-axis with $-1.4\% < \delta < 1.4\%$ (Table 4). 1000-turn ray-tracing. Fringe fields are set in bends and quadrupoles, sextupoles are off. Only particles with momentum dispersion $\delta \leq 1.2\ 10^{-2}$ survive.

Table 4: Momentum detuning within $-1.4\% < \delta < 1.4\%$ as obtained from Fourier transform of the 1000-turn phase space coordinates displayed in Fig. 8, and related local beta values at *SMSR*.

Momentum detuning, fringe fields set in bends and quads					
		Horizontal		Vertical	
part. #	$\delta p/p$	Q_x fractional	β_x (m) at *SMSR*	Q_y fractional	β_y (m) at *SMSR*
1	-0.014	*lost after a few hundred turns*			
2	-0.012	.514013	319.8	.547416	173.3
3	-0.01	.552079	258.6	.413817	137.2
4	-0.008	.588949	251.2	.622859	125.8
5	-0.006	.374765	248.6	.658753	120.4
6	-0.004	.338931	247.8	.694224	117.5
7	-0.002	.303460	248.6	.270586	115.9
8	0.	.268255	250.7	.235585	115.3
9	0.002	.233290	253.9	.200672	115.5
10	0.004	.198387	259.3	.165667	116.8
11	0.006	.163506	267.5	.130277	120.0
12	0.008	.128397	281.2	.093724	128.0
13	0.01	.092666	307.7	.053014	159.0
14	0.012	.092666	307.7	.053014	159.0
15	0.014	*lost after 63 turns*			

from Fourier analysis. The local horizontal closed orbit is (though negligible) not exactly zero, which is due to the fringe fields in bending magnets with perhaps some contribution of non exactly vanishing dispersion functions D_x, D'_x.

Only those particles with $|\delta| \leq 0.012$ survive 1000 turns - regardless of the meaningfulness of the betatron amplitude. Local phase space trajectories at *SMSR* are shown in Fig. 8, Table 4 gathers the related tune numbers and beta values at *SMSR*, from which the following tune derivatives can be drawn,

$$\begin{aligned} Q'_x &= -17.54, & Q'_y &= -17.48 \\ Q''_x &= 60, & Q''_y &= 22 \end{aligned} \tag{9}$$

not very different from the fringe field free case (Eq. 7, p. 6).

6 Chromaticity corrected machine

We now turn on the arc chromaticity sextupoles, other ones are not excited according to Ref. [1]. Harmon outputs from MAD, *in the absence of fringe fields*, are as follows :

MAD outputs

```
-------------------------------------------------------------------------------------------------
-------------------------------------------------------------------------------------------------
HARMON startup.              HARMON              line: SMSR                        range: #S/#E
Delta(p)/p:      .000000     symm: F             super:   1
-------------------------------------------------------------------------------------------------
Derivatives of tune w.r.t. momentum:
                h o r i z o n t a l                              v e r t i c a l
          first          second          third          first          second          third
   -8.047897E-02    3.234330E+00    4.944775E+02    8.031269E-02   -1.896759E+01   -3.014135E+02

Tune shift with amplitude:
     d(Qx)/d(Ex)     d(Qy)/(dEy)     d(Qy)/d(Ex)
    2.194047E+01    6.265941E+01   -8.797014E+01
```

With the TWISS command ("twiss, save , deltap=-.0002:.0002:.0001") :

```
Delta(p)/p:     -.000200 :
-------------------------------------------------------------------------------------------------
begin SMSR       1      .000  249.392   .000    .000  -.0006   .000   .006  .000  115.422  -.002
end   SMSR       1  2068.759  249.392   .000  11.254  -.0006   .000   .006  .000  115.422  -.002
-------------------------------------------------------------------------------------------------
total length =       2068.759047     Qx       =         11.254481     Qy       =         12.287271
delta(s)     =         -1.070274 mm  Qx'      =          -.001168     Qy'      =           .007540
alfa         =           .258638E-02

Delta(p)/p:     -.000100 :
-------------------------------------------------------------------------------------------------
begin SMSR       1      .000  249.521   .000    .000  -.0002   .000   .003  .000  115.371  -.001
end   SMSR       1  2068.759  249.521   .000  11.254  -.0002   .000   .003  .000  115.371  -.001
-------------------------------------------------------------------------------------------------
total length =       2068.759047     Qx       =         11.254468     Qy       =         12.287285
delta(s)     =          -.535124 mm  Qx'      =          -.000600     Qy'      =           .003778
alfa         =           .258650E-02
```

```
Delta(p)/p:      .000100 :
-------------------------------------------------------------------------------------------------
begin SMSR       1      .000  249.777   .000    .000  -.0002   .000  -.003  .000  115.270   .001
end   SMSR       1  2068.759  249.777   .000  11.254  -.0002   .000  -.003  .000  115.270   .001
-------------------------------------------------------------------------------------------------
total length =       2068.759047     Qx       =         11.254441     Qy       =         12.287312
delta(s)     =           .535097 mm  Qx'      =           .000628     Qy'      =          -.003796
alfa         =           .258675E-02

Delta(p)/p:      .000200 :
-------------------------------------------------------------------------------------------------
begin SMSR       1      .000  249.905   .000    .000  -.0006   .000  -.006  .000  115.220   .002
end   SMSR       1  2068.759  249.905   .000  11.254  -.0006   .000  -.006  .000  115.220   .002
-------------------------------------------------------------------------------------------------
total length =       2068.759047     Qx       =         11.254428     Qy       =         12.287324
delta(s)     =          1.070169 mm  Qx'      =           .001290     Qy'      =          -.007610
alfa         =           .258687E-02
```

Note the discrepancy on the derivatives of tunes w.r.t. momentum between Harmon results and TWISS command that gives

$$Q'_x = -0.135 \ , \qquad Q'_y = 0.135$$
$$Q''_x = -100 = -Q''_y \tag{10}$$

As to the ray-tracing, given that sextupole fringe fields are neglected the related multipole field and derivatives as used in the integration algorithm derive from the s-independent 2-D scalar potential

$$V_3(x,y) = G_3(3x^2 - y^2)y/3 \tag{11}$$

where $G_3/B\rho$ is the strength.

6.1 Fringe fields in quadrupoles only

We first turn fringe fields on in (all) quadrupoles only, not in bends.

Amplitude detuning Fig. 9-top shows phase space trajectories at *SMSR* obtained from a 1000-turn run, in the case of independent x_0 and y_0 initial conditions. The dynamic aperture with these working hypothesis still exceeds the physical acceptance. Table 5-top gathers tunes and local beta values at *SMSR* as a function of amplitude ; by comparison with Table 3 one can observe that amplitude detuning is still very small, namely,

$$dQ_x/d\epsilon_x/\pi = 137 \ , \qquad dQ_y/d\epsilon_y/\pi = 141 \tag{12}$$

Momentum detuning Fifteen particles are launched at *SMSR* for 1000-turn ray-tracing, with $-3\ 10^{-2} \leq \delta \leq 3\ 10^{-2}$, with zero initial horizontal coordinates since the local chromatic closed orbit is quasi-zero, and with very small amplitude vertical motion in order to be able to get the vertical tunes from Fourier analysis. (This is all very similar to what was done in Section 5 except for the sextupoles that are now active and for the bend fringe fields that are absent). All particles survive as illustrated in the phase space plot of Fig. 10. Table 6

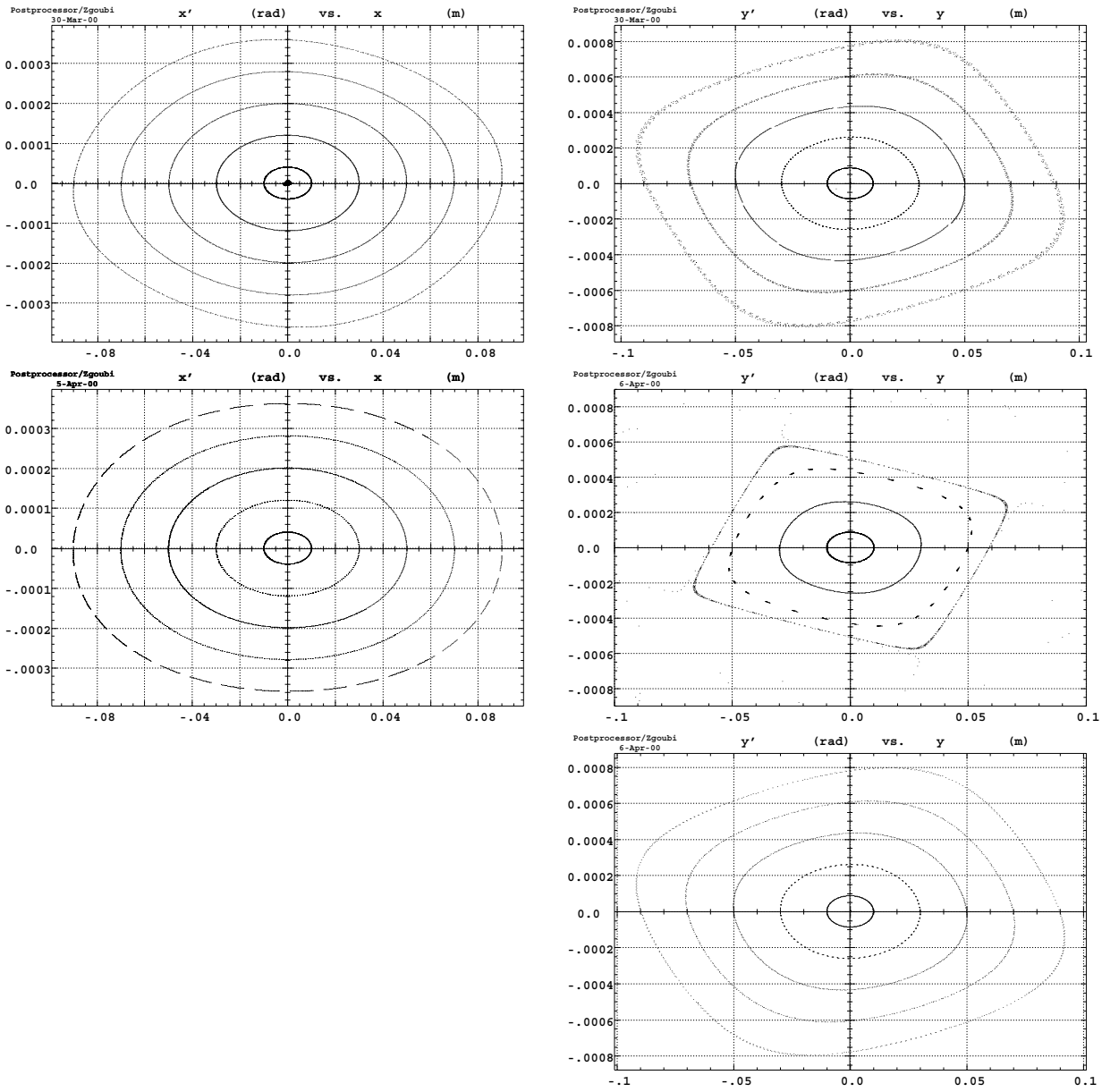

Figure 9: Phase space trajectories observed at *SMSR*. Sextupoles are on. 1000-turn ray-tracing. Initial conditions were respectively,
left : $x_0 = 1 - 9 \times 10^{-2}$m by 10^{-2}m steps and $y_0 \equiv 0$, and
right : $y_0 = 1 - 9 \times 10^{-2}$m by 10^{-2}m steps and $x_0 \equiv 0$, and in addition $y_0 = 5.9 \times 10^{-2}$m in the middle plot.
- Top row : fringe fields are set in all quadrupoles. All particles survive.
- Middle row : fringe fields are set in bends and all quadrupoles. All particles with horizontal motion survive ; vertical dynamic aperture is limited to $y_0 < 0.06$ m due to paraxial $Q_y \approx 0.24$ while $dQ_y/d\epsilon_y/\pi > 0$.
- Bottom row : the vertical acceptance, by comparison with the middle right plot, is recovered by re-tuning $Q_y(y_0 = 0)$ slightly beyond a quarter-integer value (≈ 0.279 here).

Table 5: Amplitude detuning as obtained from Fourier transform of 1000-turn phase space coordinates at *SMSR* (Fig. 9), and related beta values.

Amplitude detuning
Arc sextupoles are on

Horizontal (ϵ_y=0)			Vertical (ϵ_x=0)		
x_0 (10^{-2}m)	Q_x fractional	β_x (m)	y_0 (10^{-2}m)	Q_y fractional	β_y (m)
Fringe fields set in all quads (Fig. 9-top)					
0.001	.235071	250.8	0.001	.270009	115.2
1	.235124	250.9	1	.270132	115.2
3	.235567	250.8	3	.271032	115.1
5	.236442	250.6	5	.272643	115.2
7	.237696	250.5	7	.274602	115.2
9	.239216	250.2	9	.276145	115.3
Fringe fields set in bends and quads (Fig. 9-middle)					
0.001	.270555	250.4	0.001	.237839	115.3
1	.270610	250.5	1	.237953	115.3
3	.271088	250.3	3	.238957	115.2
5	.272017	250.1	5	.241380	115.3
-	-	-	5.9	.244467	115.4
-	-	-	6	*lost at turn # 250*	
7	.273350	250.0	7	*lost at turn # 259*	
9	.274980	249.6	9	*lost at turn # 280*	
Fringe fields set in bends and quads ** after vertical re-tuning (Fig. 9-bottom) **					
0.001	.27055	250.4	0.001	.279424	115.3
1	.27061	250.5	1	.279544	115.3
3	.27108	250.3	3	.280480	115.2
5	.27201	250.1	5	.282196	115.3
7	.27335	250.0	7	.284345	115.3
9	.27498	249.6	9	.286217	115.3

gathers the related tune numbers and beta values at *SMSR*, from which the following first and second order tune derivatives can be drawn,

$$\begin{aligned} Q'_x &= 0.015, & Q'_y &= 0.03 \\ Q''_x &= 3100, & Q''_y &= -25000 \end{aligned} \tag{13}$$

Second order is sensibly different from the fringe field free case (after MAD outputs, Eq. 10).

Table 6 also reveals momentum detuning to quarter-integer tunes in the $\delta \approx 2\ 10^{-2}$ region, that might cause some DA squeeze ; however the situation will be slightly different when fringe fields are set in bends in addition (see page 22).

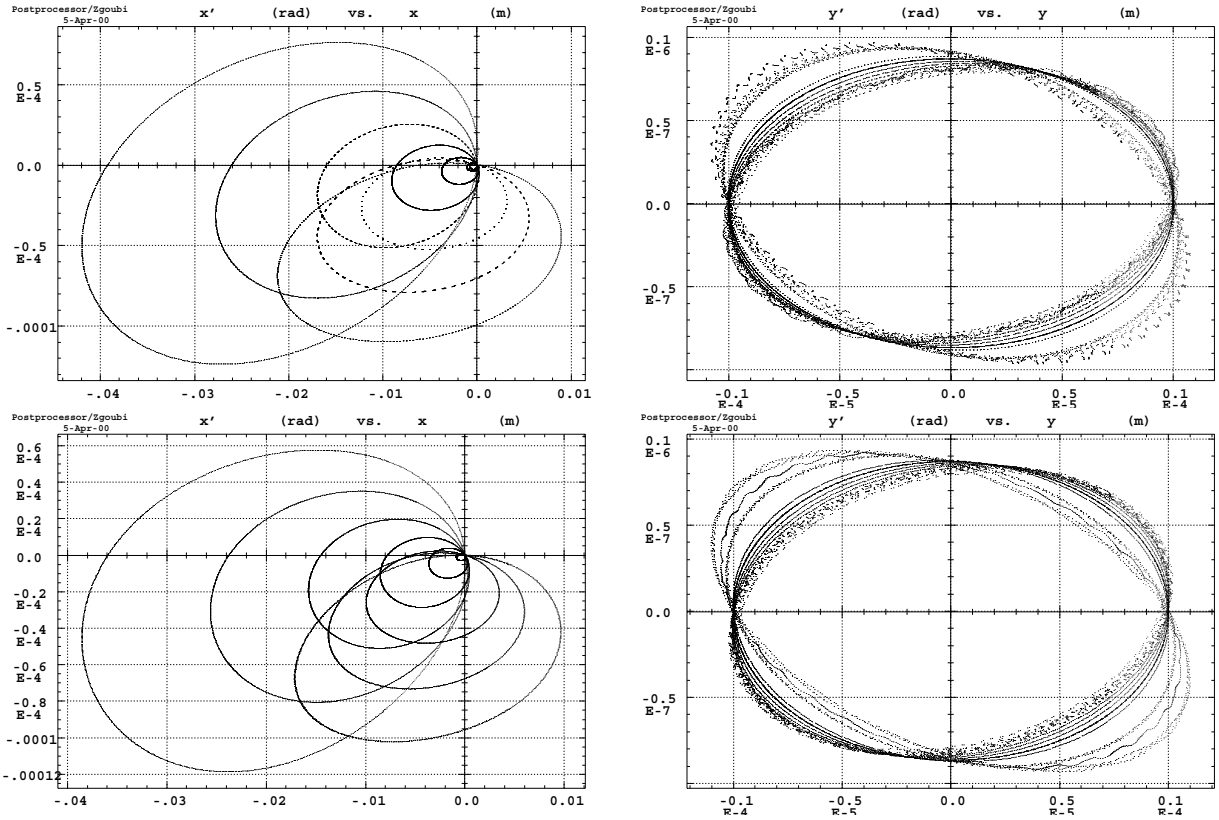

Figure 10: Horizontal (left) and vertical (right) phase space trajectories at *SMSR* of particles launched on-axis with $-3\% < \delta < 3\%$ (Table 6). Sextupoles are on. 1000-turn ray-tracing.
- Top row : fringe fields are set in all quadrupoles.
- Bottom row : fringe fields are set in bends and all quadrupoles.
All particles survive.

6.2 Fringe fields in bends and quadrupoles

Bend fringe fields are now turned on (with $\lambda_1 = 0.18$ m) together with quadrupole ones.

Table 6: Momentum detuning within $-3\% < \delta < 3\%$ as obtained from Fourier transform of the 1000-turn phase space coordinates at *SMSR* displayed in Fig. 10, and related local beta values.

Momentum detuning
Sextupoles are on

part. #	$\delta p/p$	Horizontal Q_x fractional	Horizontal β_x (m) at *SMSR*	Vertical Q_y fractional	Vertical β_y (m) at *SMSR*
Fringe fields set in all quadrupoles (Fig. 10-top)					
1	-0.03	.237527	220.1	.259573	126.1
2	-0.025	.236981	221.7	.261952	124.6
3	-0.02	.236571	225.3	.264262	123.1
4	-0.015	.236087	230.5	.266359	121.2
5	-0.01	.235569	236.8	.268125	119.3
6	-0.005	.235150	243.8	.269393	117.1
7	-10^{-4}	.235082	250.9	.270007	115.1
8	0.	.235068	251.0	.270135	115.3
9	10^{-4}	.235085	251.1	.270013	115.1
10	0.005	.235662	257.9	.269713	113.5
11	0.01	.237335	264.3	.268224	112.2
12	0.015	.240589	269.3	.265164	111.6
13	0.02	.245907	273.5	.260055	112.1
14	0.025	.253729	276.3	.252305	114.4
15	0.03	.264500	278.8	.241173	118.6
Fringe fields set in bends and all quadrupoles (Fig. 10-bottom)					
1	0.03	.291032	270.5	.200800	130.5
2	0.025	.281527	268.8	.214400	122.5
3	0.02	.275033	266.6	.223932	117.9
4	0.015	.271123	263.8	.230406	115.5
5	0.01	.269367	260.3	.234538	114.4
6	0.005	.269320	255.7	.236868	114.5
7	10^{-4}	.270515	250.6	.237831	115.2
8	0.	.270553	250.5	.237839	115.2
9	-10^{-4}	.270586	250.4	.237846	115.3
10	-0.005	.272689	245.2	.237791	116.4
11	-0.01	.275449	239.7	.237010	117.9
12	-0.015	.278633	234.5	.235723	119.3
13	-0.02	.282145	230.2	.234126	120.9
14	-0.025	.286043	226.9	.232369	122.4
15	-0.03	.290536	224.8	.230596	123.7

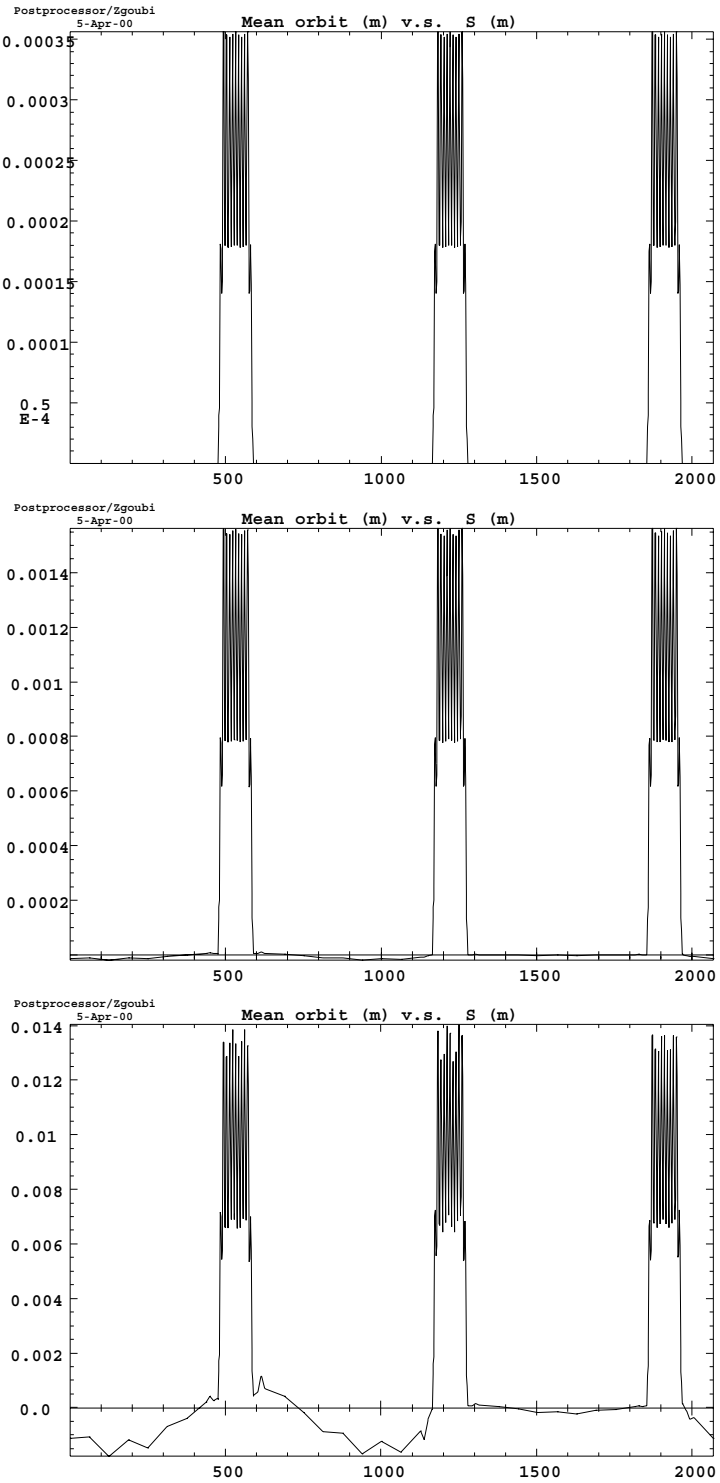

Figure 11: Chromatic closed orbit for $\delta = 10^{-4}$ (top), $\delta = 10^{-3}$ (middle) and $\delta = 10^{-2}$ (bottom). Fringe fields are set in bends and quads.

Amplitude detuning Fig. 9-middle shows phase space trajectories at *SMSR* obtained from a 1000-turn run in the case of independent x_0 and y_0 initial conditions. The horizontal dynamic aperture with these working hypothesis still exceeds the physical acceptance ; the paraxial vertical tune is obviously badly chosen considering that $dQ_y/d\epsilon_y/\pi > 0$ which brings Q_y to quarter-integer value and reduces the dynamic aperture, to about $y_{0|_{SMSR}} = 0.06$ m ($\epsilon_y/\pi \approx 31\ 10^{-6}$ m.rad) ; good situation is recovered by starting from paraxial vertical tune of about 0.28 (Table 5-bottom and Fig. 9-bottom).

Middle and bottom data in Table 5 are drawn from the data displayed in Fig. 9-middle and -bottom and give the tunes and local beta values at *SMSR* as a function of amplitude ; by comparison with Table 3 and Eq. 12 one can observe that amplitude detuning is left practically unchanged by bends fringe fields, namely

$$dQ_x/d\epsilon_x/\pi = 137\ , \qquad dQ_y/d\epsilon_y/\pi = 131 \tag{14}$$

Momentum detuning All particles survive as illustrated in Fig. 10-bottom. Related tune numbers and beta values at *SMSR* are gathered in Table 6, and the following first and second order tune derivatives can be drawn,

$$\begin{aligned} Q'_x &= -0.355\ , & Q'_y &= -0.075 \\ Q''_x &= -500\ , & Q''_y &= -100 \end{aligned} \tag{15}$$

Table 6 also reveals absence off harmful fractional integer tune in the $-3\ 10^{-2} \leq \delta \leq 3\ 10^{-2}$ range, which is favorable to DA, as corroborated by the 6-D dynamic aperture tracking that follows.

Chromatic closed orbit Fig. 11 displays the chromatic closed orbit as obtained from 100-turn pick-up signal averaging.

7 6-D dynamic aperture

Finally we launch from *SMSR* a 2000-particle beam with $x, x', z, z', \delta l, \delta p/p$ coordinates sorted at random within Gaussian distributions truncated to 4-σ, for 200-turn ray-tracing in the complete storage ring, including chromaticity sextupoles and fringe fields in all bends and quads according to the Section 6.2 study ; paraxial tunes are $Q_x = 0.2705$ and $Q_y = 0.2794$.

Final phase-spaces at *SMSR* and corresponding histograms of the coordinates are shown in Fig. 12.

All particles survive. It can be observed that, apart from expected bunch lengthening in the absence of RF system, all other coordinates have their σ-values practically unchanged, and $\epsilon_{x,z,l}$ emittances are preserved. In other words the 6-D DA again exceeds the physical acceptance.

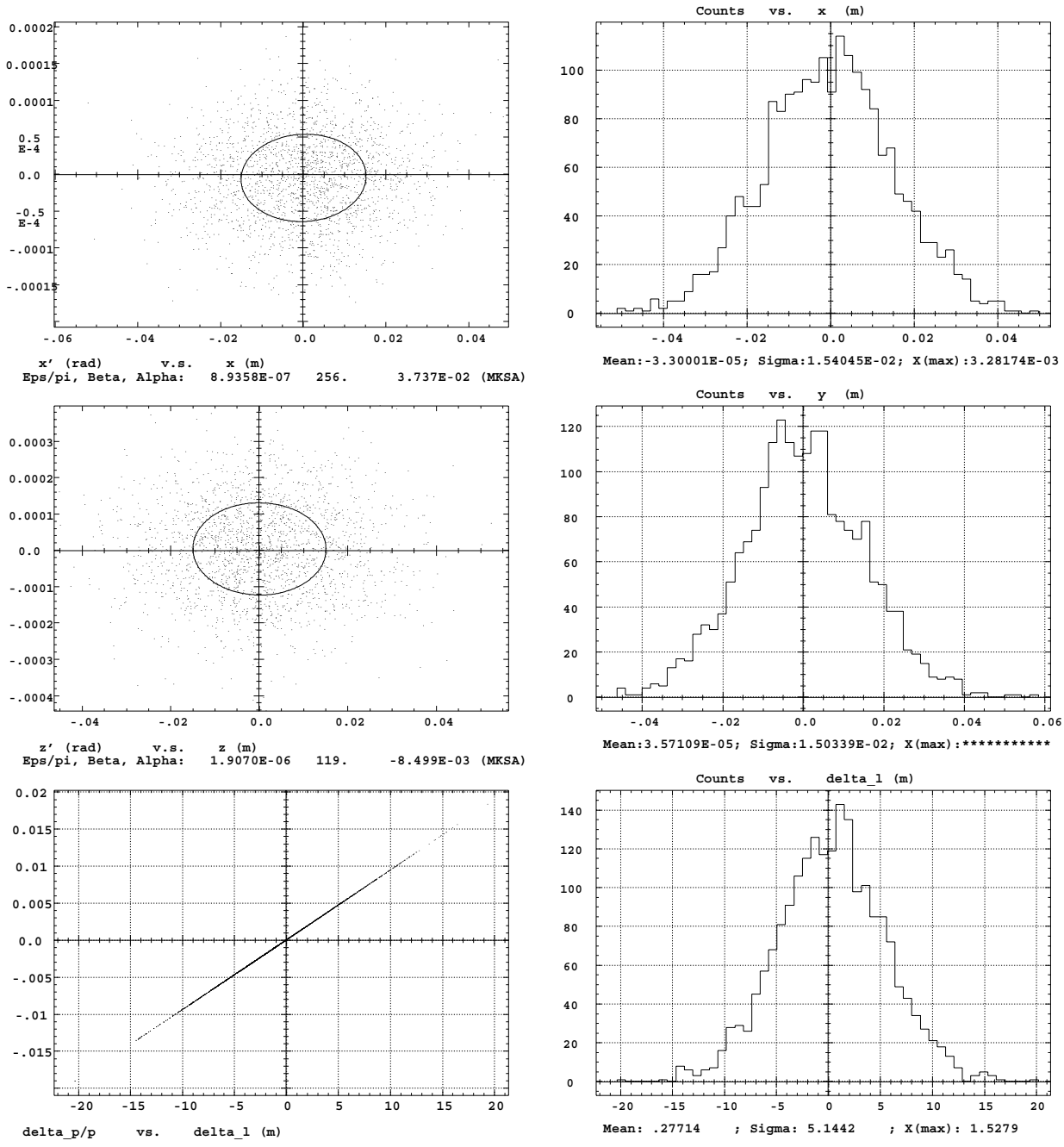

Figure 12: Properties of a 6-D 2000-particle beam after 200 turns tracking in the storage ring.
Left col. : phase spaces at *SMSR* ; right col. : corresponding histograms.
Top row : horizontal motion ; middle row : vertical motion ; bottom row : longitudinal motion.
Sextupoles are on, fringe fields are set in all bends and quads. All particles survive.

8 Comparisons with PEP magnets fringe field

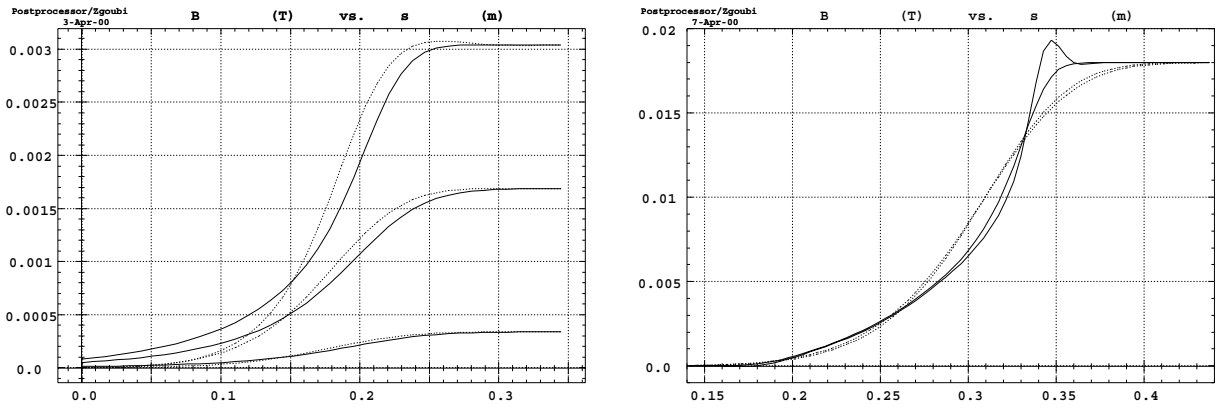

Figure 13: Left : a plot of the magnetic field experienced by a particle traversing a QFS type quadrupole with PEP magnet coefficients (Eq. 16) 1, 5, and 9 cm off axis (solid lines) together with fields of Fig. 3-right for comparison (dashed lines).
Right : field experienced 1 and 3 cm off axis in bends, in PEP case (Eq. 19, solid lines) and in GSI coefficients case (dashed lines, Eq. 8 and $\lambda_1 = 0.18$ m, see Fig. 6).

For the sake of comparison we now repeat simulations of Section 6 with the PEP type fringe field coefficients used for similar study performed with the computer code COSY [2].

8.1 Fringe fields in quadrupoles only

We first set fringe fields in quadrupoles only, with coefficients

$$C_0 = 0.296471,\ C_1 = 4.533219,\ C_2 = -2.270982,\ C_3 = 1.068627,\ C_4 = -0.036391,\ C_5 = 0.022261 \tag{16}$$

and scaling factor either $\lambda_2 = 0.178$ m in straight and matching sections or $\lambda_2 = 0.06$ m in arc quadrupoles.

As appears below things do not change substantially w.r.t. Section 6. This can be understood from the similarity of the two types of fringe fields as shown in Fig. 13 (data given in App. C), their main difference being in the abruptness of the fall-off which is however of little effect as already observed in Table 3.

Amplitude detuning Fig. 14-top shows phase space trajectories at *SMSR* obtained from a 1000-turn run, in the case of independent x_0 and y_0 initial conditions, with fringe fields set in all quadrupoles, not in bends. The dynamic aperture with these working hypothesis still exceeds the physical acceptance. Table 7 gives related amplitude detuning at *SMSR* ; comparison with Table 5 shows no fundamental difference, amplitude detunings are comparable to the GSI field case (Eq. 12).

$$dQ_x/d\epsilon_x/\pi = 250\ , \qquad dQ_y/d\epsilon_y/\pi = 25.3 \tag{17}$$

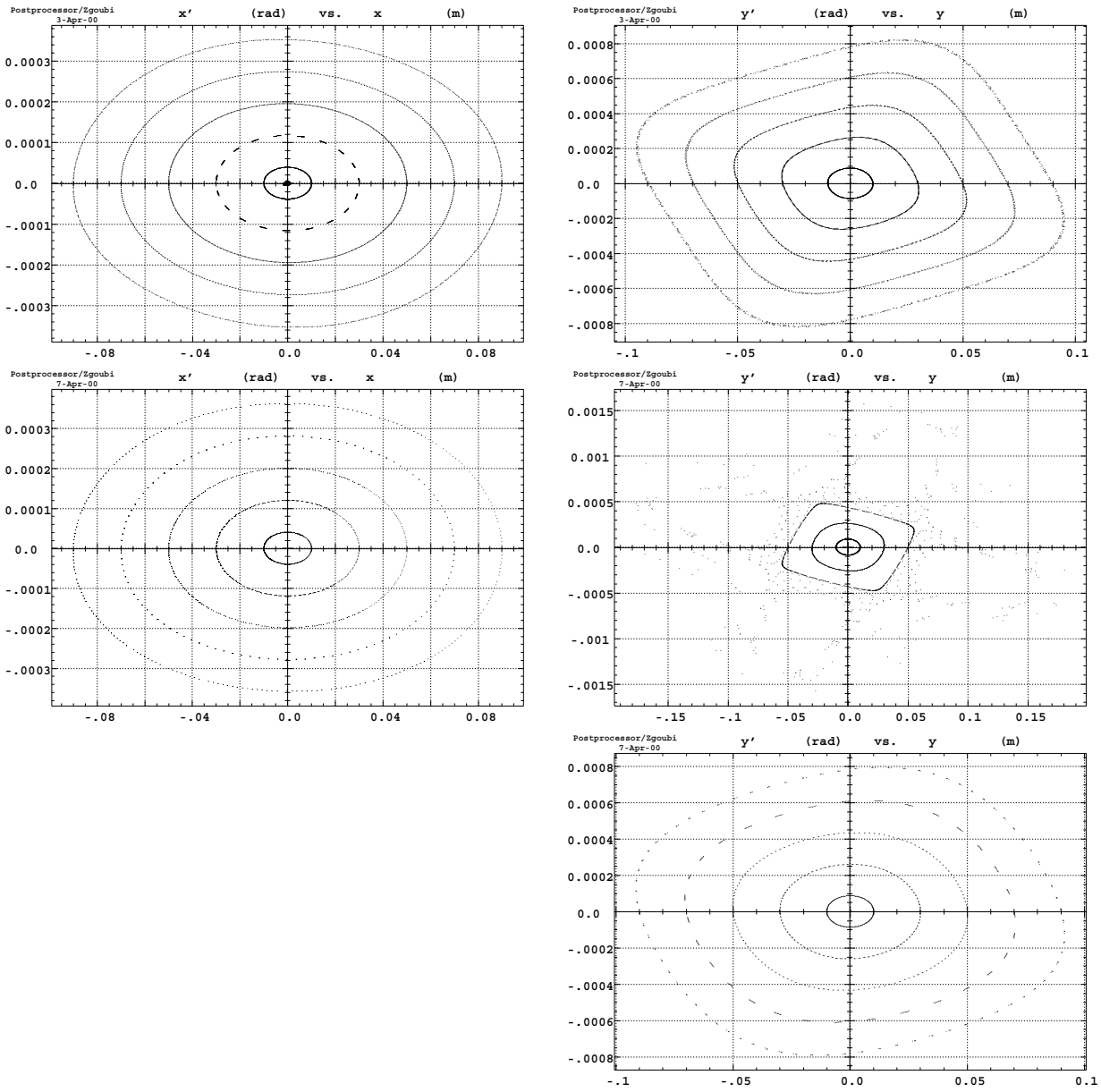

Figure 14: PEP case. Phase space trajectories observed at *SMSR*. Sextupoles are on. 1000-turn ray-tracing.
Initial conditions were respectively,
left : $x_0 = 1 - 9 \times 10^{-2}$m by 10^{-2}m steps and $y_0 = 0$, and
right : $y_0 = 1 - 9 \times 10^{-2}$m by 10^{-2}m steps and $x_0 \equiv 0$, and in addition $y_0 = 5.9 \times 10^{-2}$m in the middle plot.
- Top row : fringe fields are set in all quadrupoles. All particles survive.
- Middle row : fringe fields are set in bends and all quadrupoles. All particles with horizontal motion survive ; vertical dynamic aperture is limited to $y_0 < 0.06$ m due to paraxial $Q_y \approx 0.24$ while $dQ_y/d\epsilon_y/\pi > 0$.
- Bottom row : the vertical acceptance, by comparison with the middle right plot, is recovered by re-tuning $Q_y(y_0 = 0)$ slightly beyond a quarter-integer value (≈ 0.279 here).

Table 7: PEP type coefficients. Amplitude detuning as obtained from Fourier transform of 1000-turn phase space coordinates at *SMSR* (Fig. 14).

Amplitude detuning Arc sextupoles are on			
Horizontal ($\epsilon_y = 0$)		Vertical ($\epsilon_x = 0$)	
x_0 (10^{-2}m)	Q_x fractional	y_0 (10^{-2}m)	Q_y fractional
Fringe fields set in quadrupoles (Fig. 14-top)			
0.001	.241199	0.001	.276058
1	.24130	1	.27608
3	.24227	3	.27625
5	.24419	5	.28136
7	.24711	7	.28696
9	.25102	9	.29302
Fringe fields set in bends and all quadrupoles			
$\lambda_1 = 0.06$ *m (Fig. 14-middle)*			
0.001	.273968	0.001	.241141
1	.274053	1	.241304
3	.274751	3	.242692
5	.276157	5	.250099
7	.278259	7	.250026
9	.281022	9	.249952
$\lambda_1 = 0.12$ *m*			
0.001	.273444	0.001	.239576
1	.273534	1	.239736
3	.274232	3	.241107
5	.275631	5	.245638
7	.277718	7	.263024
9	.280473	9	.249801
$\lambda_1 = 0.06$ *m*			
* *after vertical re-tuning (Fig. 14-bottom)* *			
0.001	.273968	0.001	.282740
1	.274053	1	.282899
3	.274751	3	.284194
5	.276157	5	.286721
7	.278259	7	.290346
9	.281022	9	.294864

Momentum detuning Working conditions are the same as in Section 6.1 except for the PEP fringe fields (Eq. 16) set in quadrupoles (no fringe fields in bends here). Phase space trajectories are very similar to those obtained with the GSI quadrupole coefficients as displayed in Fig. 10, in particular all particles within the explored range $-3\% < \delta p/p < 3\%$ do survive 1000 turns. Table 8 gives the tunes vs. momentum deviation δ, showing little

Table 8: Momentum detuning with the PEP type fringe field coefficients.

Momentum detuning, PEP fringe fields set in quads, arc sextupoles on			
part. #	$\delta p/p$	Q_x fractional	Q_y fractional
1	-0.03	.241426	.268630
2	-0.025	.245856	.269066
3	-0.02	.244990	.270841
5	-0.01	.242079	.274412
6	-0.005	.241391	.275563
7	-10^{-4}	.241197	.276055
8	0.	.241199	.276058
9	10^{-4}	.241202	.276060
10	0.005	.241749	.275705
11	0.01	.243547	.274194
13	0.02	.253524	.266058
14	0.025	.261920	.258606
15	0.03	.270407	.248601

difference with previous results in Table 6, with in particular (not very different from the GSI fringe field case, Eq. 13)

$$Q'_x \approx Q'_y \approx 0.025$$
$$Q''_x \approx 2592 \approx -Q''_y \tag{18}$$

8.2 Fringe fields in bends and quadrupoles

We now add fringe fields in bends,

$$C_0 = 0.478959,\ C_1 = 1.911289,\ C_2 = -1.185953,\ C_3 = 1.630554,\ C_4 = -1.082657,\ C_5 = 0.318111 \tag{19}$$

with scaling factor $\lambda_1 = 0.062$ m.

Amplitude detuning Fig. 14-middle shows phase space trajectories at *SMSR* obtained from a 1000-turn run. Harmfulness of vertical quarter-integer tune again appears clearly, yet the dynamic aperture still exceeds the physical acceptance with adequate working point (Fig. 14-bottom). Table 7 gives the related amplitude detuning at *SMSR* ; comparison with Table 5 shows no fundamental difference, amplitude detunings are of similar amount.

9 Conclusion

A detailed study of the effects of quadrupole and/or bend fringe fields in the 50 GeV muon storage ring CERN design shows their innocuousness in terms of geometrical and momentum

acceptance, at least within the limits of the physical aperture of the vacuum chamber, as long as tune working regions are chosen far enough from resonances these fringe fields are likely to excite. A 2000-particle 6-D tracking allows to conclude that the 200-turn dynamical aperture is beyond physical acceptance and beyond $\pm 3\%$ momentum acceptance.

It has been shown that prohibitive harmful effects (detuning, acceptance reduction) are induced by too strong longitudinal fringe field gradients, which suggests preliminary design of reasonably smooth quad and bend field fall-offs over the all physical acceptance, prior to dynamic aperture evaluations.

The results exposed here have been corroborated in a recent publication on the topic [13].

Acknowledgments

Useful discussions with A. Tkatchenko (IPN Orsay) and F. Zimmermann (CERN) have enlightened various aspects of the problem.

Appendix

A MAD data file

```
TITLE &
"50 GeV 15mm 6T .5 percent muon storage ring lattice for nu factory"
!
! DATE AND TIME:    16/02/00  15.34.31
!
! FILE:             feb14b.sav
!
QFA: QUADRUPOLE, L=QUADL, K1=K1QFA
QFA2: QUADRUPOLE, L=QUADL/2.0, K1=QFA[K1]
QDA: QUADRUPOLE, L=QUADL, K1=K1QDA
QDA2: QUADRUPOLE, L=QUADL/2.0, K1=K1QDA
LA: DRIFT, L=FREES/2.0
! SFA: SEXTUPOLE, L=SEXTL, K2=1.18418285921
! SDA: SEXTUPOLE, L=SEXTL, K2=-2.120690878832
SFA: SEXTUPOLE, L=SEXTL, K2=2.848263
SDA: SEXTUPOLE, L=SEXTL, K2=-5.061285
LSA: DRIFT, L=FREES/6.0
BA:RBEND,L=DIPOLEL,ANGLE=6.28318530718/(4.0*SUPERN*(V1+V2)+&
2.0*(PERIODN-2.0*SUPERN))
BD1: RBEND, L=DIPOLEL, ANGLE=V1*6.28318530718/(4.0*SUPERN*(V1&
+V2)+2.0*(PERIODN-2.0*SUPERN))
BD2: RBEND, L=DIPOLEL, ANGLE=V2*6.28318530718/(4.0*SUPERN*(V1&
+V2)+2.0*(PERIODN-2.0*SUPERN))
SFD1: SEXTUPOLE, L=SEXTL, K2=0.0
SDD1: SEXTUPOLE, L=SEXTL, K2=0.0
SFD2: SEXTUPOLE, L=SEXTL, K2=0.0
SDD2: SEXTUPOLE, L=SEXTL, K2=0.0
COLA: RCOLLIHATOR, XSIZE=VACUUHA, YSIZE=VACUUHA
H1: HARKER
H2: HARKER
H3: HARKER
H4: HARKER
QFS: QUADRUPOLE, L=QUADSL, K1=K1QFS
QFS2: QUADRUPOLE, L=QUADSL/2.0, K1=K1QFS
QDS: QUADRUPOLE, L=QUADSL, K1=K1QDS
QDS2: QUADRUPOLE, L=QUADSL/2.0, K1=K1QDS
LS: DRIFT, L=PERIODS/2.0-QUADSL
H5: HARKER
H6: HARKER
COLS: RCOLLIHATOR, XSIZE=STRAIGHTAX, YSIZE=STRAIGHTAX
Q1H: QUADRUPOLE, L=1.0, K1=.107462886577
Q1H2: QUADRUPOLE, L=Q1H[L]/2.0, K1=Q1H[K1]
Q2H: QUADRUPOLE, L=1.0, K1=-.079510501716
Q3H: QUADRUPOLE, L=1.0, K1=.078689174539
Q4H: QUADRUPOLE, L=1.0, K1=-.048728103084
LH: DRIFT, L=11.0
QFT: QUADRUPOLE, L=QUADSL, K1=K1QFT
QFT2: QUADRUPOLE, L=QUADSL/2.0, K1=K1QFT
QDT: QUADRUPOLE, L=QUADSL, K1=K1QDT
QDT2: QUADRUPOLE, L=QUADSL/2.0, K1=K1QDT
H7: HARKER
H8: HARKER
COLT: RCOLLIHATOR, XSIZE=STRAIGHTAX, YSIZE=STRAIGHTAX
Q1HT: QUADRUPOLE, L=1.0, K1=.135813017719
Q1HT2: QUADRUPOLE, L=Q1HT[L]/2.0, K1=Q1HT[K1]
Q2HT: QUADRUPOLE, L=1.0, K1=-.083868794374
Q3HT: QUADRUPOLE, L=1.0, K1=.078498014165
Q4HT: QUADRUPOLE, L=1.0, K1=-.049609904754
LHT: DRIFT, L=11.0

CA: LINE=(LSA,SFA,LSA,BA,LA,QDA,LSA,SDA,LSA,BA,LA,QFA)
CD: LINE=(LSA,SFD1,LSA,BD1,LA,QDA,LSA,SDD1,LSA,BD1,LA,QFA,&
 LSA,SFD2,LSA,BD2,LA,QDA,LSA,SDD2,LSA,BD2,LA)

BARARC: LINE=(H3,CD,QFA,H1,CA,H2,7*CA,-CD,H4)

ARC: LINE=(QFA2,BARARC,QFA2)
CS: LINE=(LS,QDS,LS,QFS)
HC: LINE=(Q1H,LH,Q2H,LH,Q3H,LH,Q4H)
CT: LINE=(LS,QDT,LS,QFT)
HT: LINE=(Q1HT,LHT,Q2HT,LHT,Q3HT,LHT,Q4HT)
BARCT: LINE=(LS,QFT,3*CT,LS)
ST: LINE=(HT,BARCT,-HT)
BARCS: LINE=(LS,QFS,3*CS,LS)
SP: LINE=(HC,BARCS,-HC,BARARC)
HUSR: LINE=(2*SP,HT,BARCT,-HT,BARARC)
SHSR: LINE=(COLS,QFS2,3*CS,LS,m1, &
-HC,m2,BARARC,SP,HT,BARCT,-HT,BARARC,HC,LS,QFS2)

COLLPC := 50.0
EPSXN := .16667E-2
SIGE := .5E-2
SUPERN := 3.0
SIGN := 3.0
HU2PI := .25
PERIODN := 30.0
PERIODL := 9.702986212739
DIPOLEL := 2.910895863822
FOCALL := 3.430523674394
! arc quad length :
QUADL := .49966360797
FREES := 1.440933634577
VACUUHA := .030832596093
PERIODS := 1.25E2
HUS2PI := .120077386989
FOCALS := 84.837654817115
! LSS quad length :
QUADSL := .349822107399
STRAIGHTAX := .088972667089
K1QFA := .603714246067
K1QDA := -.596691016804
SEXTL := FREES/6.0
V1 := .499822256506
V2 := .501509758147
QX := 11.254454627308
QY := 12.287298477488
QS := 0.0
QX' := -10.186528066851
QY' := -10.116220425119
ALFX := .105069985977E-12
ALFY := -.156517788234E-13
BETX := 2.496490887405E2
BETY := 1.153206713276E2
XO := 0.0
PXO := 0.0
YO := 0.0
PYO := 0.0
TO := 0.0
PTO := 0.0
AX := .79043167253E-5
AY := -.192733028301E-2
BX := 16.242555487207
BY := 2.888490954096
K1QFS := .033757938762
K1QDS := -.033757938763
K1QFT := .044393395581
K1QDT := -.045746958309
HUXT2PI := HUS2PI+.038
HUYT2PI := HUS2PI+.049
DPS := .015
! RETURN !
```

B Zgoubi data file

A translation of the MAD file of App. A to Zgoubi format.

```
50 GeV 15mm 6T .5 percent muon storage ring lattice for nu f
'OBJET'
        1000.000000
5
.001 .001 .001 .001 .0 .00001
0. 0. 0. 0. 0. 1.
'HULTIPOL' QUAD      QFS2
0  .Quad
   17.4911  10.00     .0     .0337579388  .0 .0 .0 .0 .0 .0 .0 .0
.0 .0  1.00 0.00 0.00 0.00 0.00 0. 0. 0. 0.
 6  .1122 6.2671 -1.4982 3.5882 -2.1209 1.723
17.0 20.0  1.00 0.00 0.00 0.00 0.00 0. 0. 0. 0.
 6  .1122 6.2671 -1.4982 3.5882 -2.1209 1.723
 0. 0. 0. 0. 0. 0. 0. 0. 0. 0.
8.040E10  Quad  *QFS
1 0. 0. 0.
'DRIFT'    DRIF      LS
   6215.0178
'HULTIPOL' QUAD      QDS
0  .Quad
   34.9822 10.00     .0    -.0337579388  .0 .0 .0 .0 .0 .0 .0 .0
17.0 20.0  1.00 0.00 0.00 0.00 0.00 0. 0. 0. 0.
 6  .1122 6.2671 -1.4982 3.5882 -2.1209 1.723
17.0 20.0  1.00 0.00 0.00 0.00 0.00 0. 0. 0. 0.
 6  .1122 6.2671 -1.4982 3.5882 -2.1209 1.723
 0. 0. 0. 0. 0. 0. 0. 0. 0. 0.
8.040E10  Quad  *QDS
1 0. 0. 0.
'DRIFT'    DRIF      LS
   6215.0178
'HULTIPOL' QUAD      QFS
0  .Quad
   34.9822 10.00     .0     .0337579388  .0 .0 .0 .0 .0 .0 .0 .0
17.0 20.0  1.00 0.00 0.00 0.00 0.00 0. 0. 0. 0.
 6  .1122 6.2671 -1.4982 3.5882 -2.1209 1.723
17.0 20.0  1.00 0.00 0.00 0.00 0.00 0. 0. 0. 0.
 6  .1122 6.2671 -1.4982 3.5882 -2.1209 1.723
 0. 0. 0. 0. 0. 0. 0. 0. 0. 0.
8.040E10  Quad  *QFS
1 0. 0. 0.
. . . . . .
. . . . . .
. . . . . .
'DRIFT'    DRIF      LS
   6215.0178
'HULTIPOL' QUAD      Q4H
0  .Quad
  100.0000 10.00     .0    -.0487281031  .0 .0 .0 .0 .0 .0 .0 .0
17.0 20.0  1.00 0.00 0.00 0.00 0.00 0. 0. 0. 0.
 6  .1122 6.2671 -1.4982 3.5882 -2.1209 1.723
17.0 20.0  1.00 0.00 0.00 0.00 0.00 0. 0. 0. 0.
 6  .1122 6.2671 -1.4982 3.5882 -2.1209 1.723
 0. 0. 0. 0. 0. 0. 0. 0. 0. 0.
40.040E10  Quad  Q4H
1 0. 0. 0.
'DRIFT'    DRIF      LHB
   1100.0000
'HULTIPOL' QUAD      Q3H
0  .Quad
  100.0000 10.00     .0     .0786891745  .0 .0 .0 .0 .0 .0 .0 .0
17.0 20.0  1.00 0.00 0.00 0.00 0.00 0. 0. 0. 0.
 6  .1122 6.2671 -1.4982 3.5882 -2.1209 1.723
17.0 20.0  1.00 0.00 0.00 0.00 0.00 0. 0. 0. 0.
 6  .1122 6.2671 -1.4982 3.5882 -2.1209 1.723
 0. 0. 0. 0. 0. 0. 0. 0. 0. 0.
40.040E10  Quad  Q3H
1 0. 0. 0.
. . . . . .
. . . . . .
. . . . . .
'HULTIPOL' SEXT      SFA
0  .Sext
   24.0156 10.00     .00     .00 14.241315E-2  .0 .0 .0 .0 .0 .0 .0
0.00 0.00  1.00 0.0 .0 0.0 .0 0.0 .0 0.0 .0
 6  .1122 6.2671 -1.4982 3.5882 -2.1209 1.723
0.00 0.00  1.00 0.0 .0 0.0 .0 0.0 .0 0.0 .0
 6  .1122 6.2671 -1.4982 3.5882 -2.1209 1.723
 0. 0. 0. 0. 0. 0. 0. 0. 0. 0.
10.010E10  Sext  SFA
1 0. 0. 0.
'DRIFT'    DRIF      LSA
     24.0156
'HULTIPOL' RBEN      BA
0  .Dip
 290.9567  10.00     .35965512     .0 .0 .0 .0 .0 .0 .0 .0 .0
 18.00 18.00  0.00 0.00 0.00 0.00 0.00 0. 0. 0. 0.  BEND
6  .1122 6.2671 -1.4982 3.5882 -2.1209 1.723  BEN
 18.00 18.00  0.00 0.00 0.00 0.00 0.00 0. 0. 0. 0.  BEND
6  .1122 6.2671 -1.4982 3.5882 -2.1209 1.723  BEN
 0. 0. 0. 0. 0. 0. 0. 0. 0. 0.
 40.020E10    Dip  BA
          3 0.     .0E+00    .0E+00
'DRIFT'    DRIF      LA
     72.0467
'HULTIPOL' QUAD      QDA
0  .Quad
   49.9664 10.00     .0  -.5966910168  .0 .0 .0 .0 .0 .0 .0 .0
  9.0 9.0  1.00 0.00 0.00 0.00 0.00 0. 0. 0. 0. arcQ
 6  .1122 6.2671 -1.4982 3.5882 -2.1209 1.723
  9.0 9.0  1.00 0.00 0.00 0.00 0.00 0. 0. 0. 0. arcQ
 6  .1122 6.2671 -1.4982 3.5882 -2.1209 1.723
 0. 0. 0. 0. 0. 0. 0. 0. 0. 0.
20.020E10  Quad  *QDA
1 0. 0. 0.
'DRIFT'    DRIF      LSA
     24.0156
'HULTIPOL' SEXT      SDA
0  .Sext
   24.0156 10.00  .00  .00  -25.306425E-2  .0 .0 .0 .0 .0 .0 .0
0.00 0.00  1.00 0.0 .0 0.0 .0 0.0 .0 0.0 .0
 6  .1122 6.2671 -1.4982 3.5882 -2.1209 1.723
0.00 0.00  1.00 0.0 .0 0.0 .0 0.0 .0 0.0 .0
 6  .1122 6.2671 -1.4982 3.5882 -2.1209 1.723
 0. 0. 0. 0. 0. 0. 0. 0. 0. 0.
10.010E10  Sext  SDA
1 0. 0. 0.
'DRIFT'    DRIF      LSA
     24.0156
. . . . . .
. . . . . .
. . . . . .
 etc...
```

C Fringe fields in bends with GSI and PEP coefficients

Data relative to Fig. 13.

```
'HULTIPOL' RBEN      BD1             GSI coeffs
 2 .Dip
 50.0  10.00     .17976363     .0  .0 .0  .0  .0  .0  .0  .0  .0
  30.00 18.00  0.00 0.00 0.00 0.00 0.00 0. 0. 0. 0.  BEND
6  .1122 6.2671 -1.4982 3.5882 -2.1209 1.723  BEN
  00 00  0.00 0.00 0.00 0.00 0.00 0. 0. 0. 0.  BEND
6  .1122 6.2671 -1.4982 3.5882 -2.1209 1.723  BEN
 0. 0. 0. 0. 0. 0. 0. 0. 0. 0.
 40.140E10    Dip  BD1
          3 0.     .0000000000E+00    .0000000000E+00
'HULTIPOL' RBEN      BD1             PEP coeffs
 2 .Dip
 50.0  10.00     .17976363     .0  .0 .0  .0  .0  .0  .0  .0  .0
  30.0 6.2  1.00 0.00 0.0.0 0 0.00 0.00 0.00 0. 0. 0.  BEND
6  0.478959 1.911289 -1.185953 1.630554 -1.082657 0.318111
   .0 0.  1.00 0.00 0.0.0 0 0.00 0.00 0.00 0. 0. 0.  BEND
6  0.478959 1.911289 -1.185953 1.630554 -1.082657 0.318111  BEN
 0. 0. 0. 0. 0. 0. 0. 0. 0. 0.
 40.140E10    Dip  BD1
          3 0.     .0000000000E+00    .0000000000E+00
'END'
```

D Remarks on the design of fringe fields

Fig. 15 has been obtained with the same $C_0 - C_5$ coefficients as used in the text (Eq. 8), yet with sensibly smaller value of the scaling coefficient λ_2. It shows how strongly the off-axis field can be distorded in the quadrupole end regions in presence of abrupt end field model $\alpha_{2,0}$: the field is smooth at 1 cm, undergoes a slight negative overshoot at 5 cm,

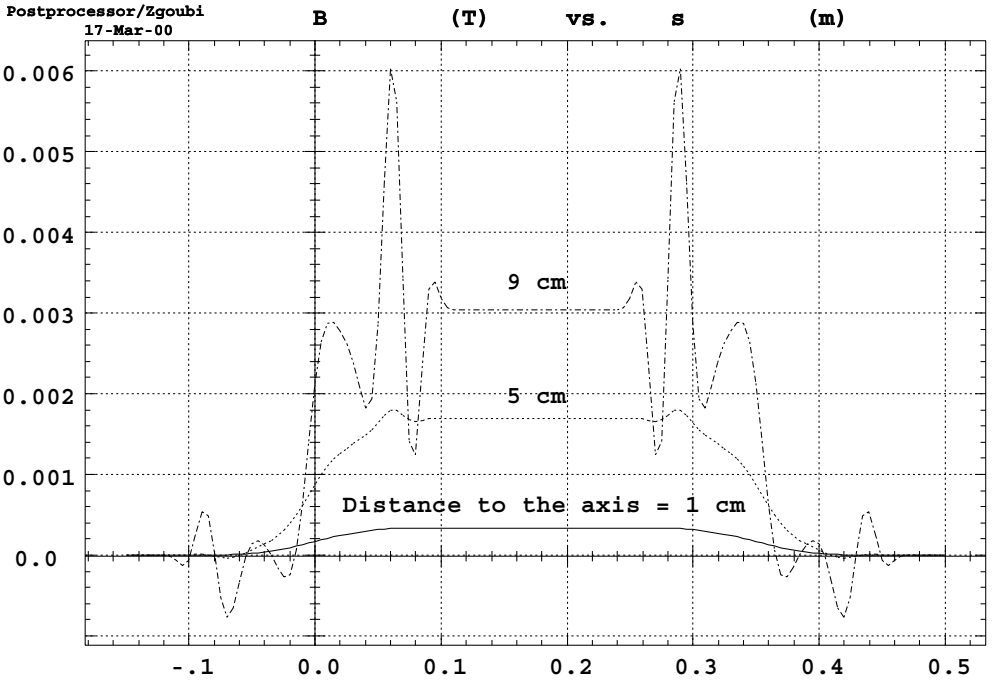

Figure 15: A plot of the magnetic field experienced by a particle traversing a QFS type quadrupole 1, 5, and 9 cm off axis.

and series of strong overshoots at 9 cm liable to cause dramatic kick $\Delta x' = \Delta x \int G\, ds/B\rho$. The immediate consequence is a sensible squeeze of the dynamic aperture down to ≈ 5 cm in both planes at *SMSR* as shown in Fig. 16 that can be compared to Fig. 4-top (page 9). This was cause of the strong DA squeeze first observed in Ref. [2].

Those considerations argue in favor of preliminary 3-D magnet simulations, in particular to assess the adequacy of fringe field coefficient values with off-axis extrapolation, prior to estimating effects of fringe field on dynamics ; conversely, in designing the quadrupoles it should be thought, if necessary, of shaping the iron or coil ends in such a way as to insure smooth field fall-offs (such as in Figs. 6, 13) within the whole physical aperture.

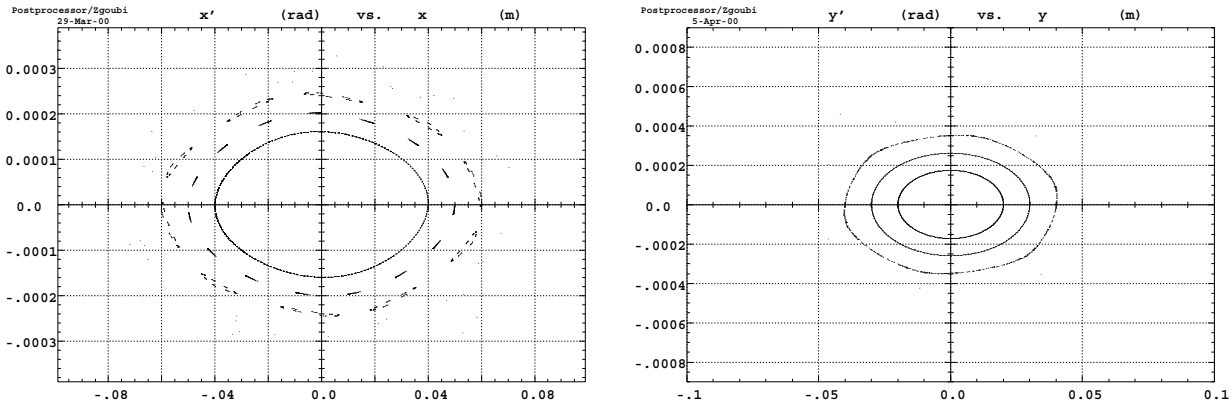

Figure 16: Phase space trajectories observed at *SMSR* in presence of fringe field of Fig. 15 set in all quadrupoles. Sextupoles are off. 1000-turn ray-tracing. Initial conditions were respectively,
left : $x_0 = 1 - 9 \times 10^{-2}$m and $\epsilon_y = 0$ (unstable motion for $x_0 \geq 0.07$ m) and,
right : $y_0 = 1 - 9 \times 10^{-2}$m and $\epsilon_x = 0$ (unstable motion for $y_0 \geq 0.05$ m).

References

[1] E. Keil, A 50 GeV muon storage ring design, Preliminary draft report, CERN, 12/03/2000, private communication.

[2] F. Zimmermann, C. Johnstone, M. Berz, B. Erdelyi, K. Makino, W. Wan, Fringe fields and dynamic aperture in muon storage rings, Draft report, FNAL, 7 March 2000, private communication.

[3] H. Grote, F. C. Iselin, The MAD Program, User's Reference Manual, CERN/SL/90-13 (AP) (Rev. 5), CERN, 29 April 1996.

[4] F. Méot and S. Valéro, Zgoubi users' guide, Report CEA/DSM/DAPNIA/SEA-97-13, Saclay, Oct. 1997.

[5] F. Méot, The ray-tracing code Zgoubi, NIM A 427 (1999) 353-356.

[6] F. Méot, A numerical method for the ray-tracing of polarized beams, Proc. EPAC Conf., 1992 ; F. Méot, A. París, Concerning effects of fringe fields and longitudinal distribution of $\mathbf{b_{10}}$ in LHC low-β regions, Report FERMILAB-TM-2017, February 2, 1998.

[7] F. Méot, On the effects of fringe fields in the LHC ring, Part. acc., 1996, Vol. 55, pp.[329-338]/83-92.

[8] F. Méot, On the effects of fringe fields in the recycler ring, Report FERMILAB-TM-2016, April 15, 1997.

[9] G. Leleux, Compléments sur la physique des accélérateurs, DEA de Physique et Technologie des Grands Instruments, rapport CEA/DSM/LNS/86-101, CEA, Saclay (1986).

[10] H.A. Enge, Deflecting magnets, in *Focusing of charged particles*, volume 2, A. Septier ed., Academic Press, New-York and London (1967).

[11] P. Senger et als., The kaon spectrometer at SIS, Report GSI-92-77, Dec. 1992.

[12] G. Leleux, Influence of quadrupole fringe fields on wave numbers, Tech. report 6-67/GL-FB, LAL, Orsay (2 Feb. 1967).

[13] F. Zimmermann, Fringe fields, dynamic aperture and transverse depolarisation in the CERN muon storage rings, CERN-SL-2000-012 AP (May 4, 2000).